Composites Science and Technology 86 (2013) 76–81

Contents lists available at SciVerse ScienceDirect

Composites Science and Technology

journal homepage: www.elsevier.com/locate/compscitech

Cured shape and snap-through of bistable twisting hybrid [0/90/metal]$_T$ laminates

Fuhong Dai *, Hao Li, Shanyi Du

Center for Composite Materials and Structures, Harbin Institute of Technology, Harbin 150001, China

ARTICLE INFO

Article history:
Received 26 June 2012
Received in revised form 3 June 2013
Accepted 30 June 2013
Available online 13 July 2013

Keywords:
A. Hybrid composites
A. Laminate
A. Smart materials
B. Non-linear behavior
C. Residual stress

ABSTRACT

This paper presents a bistable twisting CFRP-metal hybrid laminate which has an external isotropic metallic layer. Different from the pure unsymmetric CFRP laminate and the hybrid unsymmetric laminate with an inner metallic layer, the laminate presented can be transformed from one negative curvature to another negative curvature instead of from one negative curvature to another positive curvature. Their room temperature shapes can be a unique paraboloid shape, a twisted cylindrical shape, or a twisted cylindrical shape that can be snapped through to another twisted cylindrical shape. The cured shape of the hybrid laminate is studied using analytical, finite element and experimental techniques. The investigation is focused on the hybrid laminate with lay-up of [0/90/metal]$_T$, and shows that the principal direction of cured curvature is 45°. The predicted cured shape and the snap-through loads agree well with experimental results.

1. Introduction

Bistable composite laminates have been proposed to generate novel morphing and deployable structures within a range of engineering sectors [1–5]. The advantage of this approach is that while energy must be expended to snap the structure between states, no energy is required to hold the structure in the new state. For decades of years, the cured curvature of bistable laminates have been predicted with good precision by using analytical approaches [6–9]. In addition, finite element analysis has been developed as a robust way to predict cured shape and to simulate the snap through process [10,11]. The factors influencing the cured shape and bistable behaviors of unsymmetric laminates, including slippage [12], imperfection [13], fiber orientation [14], moisture [15,16] and aspect ratio [17,18], have been investigated. To induce the snap-through process from one stable state to another, the actuator materials such as shape memory alloy and piezoelectric composites have been employed [19–22]. The interests have been recently extended to study the dynamic behavior of bistable laminates as well [23,24]. The low load carrying capability and restrictive geometries of such pure composite laminates are significant design limitations [25]. One interesting idea to emerge is the hybridization of unsymmetric laminates that can give more design freedom of cured curvatures and snapping load [26,27].

Summarizing the work in open literature, several types of cured shapes of unsymmetric laminates after cooling down can be found: saddle and two cylindrical shapes for cross-ply laminate; twisted saddle and two twisted cylindrical shapes for angle-ply laminates. These laminates are either pure unsymmetric laminates or hybrid laminates with an inner orthotropic layer (CFRP-metal). They have the same feature that their cured curvatures have the opposite sign ($k_{xx} = -k_{yy}$) in two stable states.

This work presents a new bistable hybrid laminate with an external orthotropic metallic layer, whose curvatures have the same sign ($k_{xx} = k_{yy}$) in two stable states. Analytical techniques are used to carry out parametric studies of bitable hybrid laminates. These studies are verified by finite element analysis and experiments.

2. Analytical models

For unsymmetric laminates, the thermally induced directional deformation of the single layer results in large out-of-plane deformations. To take into account the large bistable deformations, the linear strain–displacement relations must be extended by non-linear terms [6,7,9,11,27]:

$$\begin{aligned}\varepsilon_x &= \varepsilon_x^0 - z\frac{\partial^2 w}{\partial x^2} = \frac{\partial u^0}{\partial x} + \frac{1}{2}\left(\frac{\partial w}{\partial x}\right)^2 - z\frac{\partial^2 w}{\partial x^2}\\ \varepsilon_y &= \varepsilon_y^0 - z\frac{\partial^2 w}{\partial y^2} = \frac{\partial v^0}{\partial y} + \frac{1}{2}\left(\frac{\partial w}{\partial y}\right)^2 - z\frac{\partial^2 w}{\partial y^2}\\ \varepsilon_{xy} &= \varepsilon_{xy}^0 - z\frac{\partial^2 w}{\partial x \partial y} = \frac{1}{2}\left(\frac{\partial u^0}{\partial y} + \frac{\partial v^0}{\partial x} + \frac{\partial w}{\partial x}\frac{\partial w}{\partial y}\right) - z\frac{\partial^2 w}{\partial x \partial y}\end{aligned} \quad (1)$$

where the index 0 refers to laminate reference plane, where u^0 and v^0 are the x- and y- reference-surface displacements, w is the z-displacement, and the ε^0s are the strains at the reference plane, ε_x, ε_y

* Corresponding author. Tel.: +86 451 86414323.
E-mail address: daifh@hit.edu.cn (F. Dai).

0266-3538/$ - see front matter © 2013 Elsevier Ltd. All rights reserved.
http://dx.doi.org/10.1016/j.compscitech.2013.06.022

and ε_{xy} the total strains. Total potential energy of the laminate are given by

$$\Pi = \int_{-L_x/2}^{L_x/2}\int_{-L_y/2}^{L_y/2}\int_{-H/2}^{H/2} \begin{pmatrix} \frac{1}{2}Q_{11}\varepsilon_x^2 + Q_{12}\varepsilon_x\varepsilon_y + Q_{16}\varepsilon_{xy}\varepsilon_x + \frac{1}{2}Q_{22}\varepsilon_y^2 + Q_{26}\varepsilon_{xy}\varepsilon_y \\ +\frac{1}{2}Q_{66}\varepsilon_{xy}^2 - (Q_{11}\alpha_x + Q_{12}\alpha_y + Q_{16}\alpha_{xy})\varepsilon_x\Delta T - \\ (Q_{12}\alpha_x + Q_{22}\alpha_y + Q_{26}\alpha_{xy})\varepsilon_y\Delta T - \\ (Q_{16}\alpha_x + Q_{22}\alpha_y + Q_{66}\alpha_{xy})\varepsilon_x\Delta T \end{pmatrix} dxdydz \quad (2)$$

where L_x and L_y are the two side-lengths of the laminate and H is the laminate thickness. In Eq. (2), Q terms represent the transformed reduced stiffness. The thermal expansion coefficient is represented by α and ΔT is temperature difference with respect to a reference state.

A practical way to solve this problem is the use of approximate expressions for both curvatures and strains-displacement relations, as functions of unknown coefficients. Generally, a solution to Eq. (2) can be obtained assuming the out-of-plane displacement, w, is of the form:

$$w(x,y) = \frac{1}{2}(ax^2 + by^2 + cxy) \quad (3)$$

where the coefficients a and b represent the curvatures in the x- and y-directions respectively in the global coordinate system. The coefficient c represents the twist curvature.

For a cross-ply $[0_n/90_n]$ or $[0_n/\text{metal}/90_n]$ laminate, the direction of principal curvature coincides with the global axes of laminate. Thus the coefficient c is zero, which can be neglected.

In contrast to the cross-ply laminate, the principal curvature's direction has an angle of θ with respect to the global axes for a laminate with lay-up of [0/90/metal], as seen in Fig. 1a. The angle θ is dependent on the fiber orientations of the single layer. It is advantageous for stability analysis to formulate the displacement in the principal curvature system and to perform a transformation into the global coordinate system according to the transformations

$$\begin{pmatrix} u \\ v \\ w \end{pmatrix} = \begin{pmatrix} \cos\theta & \sin\theta & 0 \\ -\sin\theta & \cos\theta & 0 \\ 0 & 0 & 1 \end{pmatrix} \begin{pmatrix} \bar{u} \\ \bar{v} \\ \bar{w} \end{pmatrix} \quad (4)$$

where u, v and w are x-, y- and z-displacements in the global coordinate system. $\bar{u}$, $\bar{v}$ and $\bar{w}$ are $\bar{x}$-, $\bar{y}$-and $\bar{z}$-displacement in principal curvature coordinate system.

Therefore, we use the principal curvature coordinate system to solve Eq. (2). Geometrical assumptions for the out-of-plane displacements with the general second-order approach are given by

$$\bar{w}(\bar{x},\bar{y}) = \frac{1}{2}(a_0\bar{x}^2 + b_0\bar{y}^2) \quad (5)$$

where the coefficients a_0 and b_0 define the principal curvatures of laminate in the $\bar{x}$- and $\bar{y}$-directions respectively.

For the description of the in-plane deformations, several approximations can be found in the literature. The robustness and reliability of the modeling framework depend on the scaling and conditioning number of the system of solving equations. Here, the displacements are approximated by using the following polynomials:

$$\begin{aligned} \bar{u}^0 &= a_1\bar{x} + a_2\bar{y} + a_3\bar{x}\bar{y} + a_4\bar{x}^2\bar{y} + a_5\bar{x}\bar{y}^2 + a_6\bar{x}^3 + a_7\bar{y}^3 \\ \bar{v}^0 &= b_1\bar{x} + b_2\bar{y} + b_3\bar{y}\bar{x} + b_4\bar{y}^2\bar{x} + b_5\bar{y}\bar{x}^2 + b_6\bar{y}^3 + b_7\bar{x}^3 \end{aligned} \quad (6)$$

Using the displacement approximations (5) and (6) and in the strain displacement relation (1) substituting the resulting expressions into (2), the total potential energy of laminate becomes a function dependent on the coefficients a_m,b_m (m = 0, 1, …, 7).

The principle of the minimum total potential energy requires the first variation to be zero

$$\delta\Pi = \frac{\delta\Pi}{\delta a_m}\delta a_m + \frac{\delta\Pi}{\delta b_m}\delta b_m = 0 \quad (7)$$

To satisfy this condition, every summand in Eq. (7) must be zero, which results in a coupled non-linear algebraic equation system. The equation group is solved with specially-written mathematical software. These solutions should be checked for their stability by means of $\delta^2\Pi$, which has to be positive for a stable deformation state. The basic shapes of the hybrid laminate with an external orthotropic layer are shown in Fig. 1.

Another issue about the cured shape prediction of hybrid laminates is the slippage effect. In this study, a 'slip coefficient' μ is introduced to describe slipping at the metal–fiber interface, which relies on the materials and manufacturing processes used so it must be found experimentally. We use the dimensionless slip coefficient defined by Daynes and Weaver [27]:

$$\mu = \frac{\varepsilon_f^{cure}}{\varepsilon_m^{cure}} \quad (8)$$

$$\varepsilon_m^{cure} = \frac{E_m\alpha_m\Delta T t}{\frac{\mu}{4}E_f V_f(H-t)(1-\nu_m) + E_m t} \quad (9)$$

$$\bar{\alpha}_k = \begin{Bmatrix} \mu\varepsilon_m^{cure}/2\Delta T(k=f) \\ \varepsilon_m^{cure}/\Delta T(k=m) \\ \alpha_{22}(k=r) \end{Bmatrix}$$

where ε_f^{cure} and ε_m^{cure} are the reference-plane strains at cure in the fiber and the metal layer respectively. E_f and E_m are the fiber and the metal Young's modulus. V_f is the fiber volume fraction. α_m and ν_m are the metal thermal expansion and Poisson' ratio. H is the total thickness of laminate and t is the thickness of metallic layer. The subscript f, m and r refer to the directions of fiber, the metal and the direction transverse to the fiber respectively. More details can be found in the literature [27].

3. Finite element models

The commercial finite element code ABAQUS is employed to perform the non-linear analysis. The cool-down is simulated by applying an initial temperature and a final temperature to all of the nodes of the model in first step. Then in second analysis step,

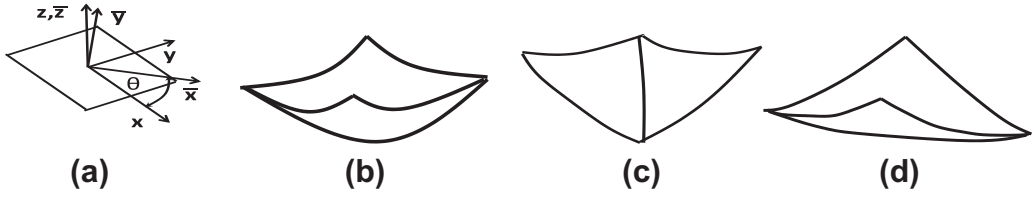

Fig. 1. Basic shapes of hybrid laminates with an external isotropic metal layer:(a) reference shape at curing temperature; (b) paraboloid shape (c) and (d) twisted cylindrical shapes at room temperature (x, y, z: global coordinate system; $\bar{x}$, $\bar{y}$, $\bar{z}$:principal curvature coordinate system).

Table 1
Thermo-mechanical properties of CFRP and metal.

CFRP	E_{11} = 126 GPa, E_{22} = 8.8 GPa, G_{12} = 4.47 GPa, v_{12} = 0.3, $\alpha_{11} = 0.25 \times 10^{-6}$/°C, $\alpha_{22} = 34 \times 10^{-6}$/°C, thickness = 0.125 mm
	E_f = 211 GPa, v_f = 0.6
Aluminum	E_m = 70 GPa, $\alpha_m = 23.6 \times 10^{-6}$/°C, thickness = 0.24 mm

Fig. 2. The illustration of imperfection regions.

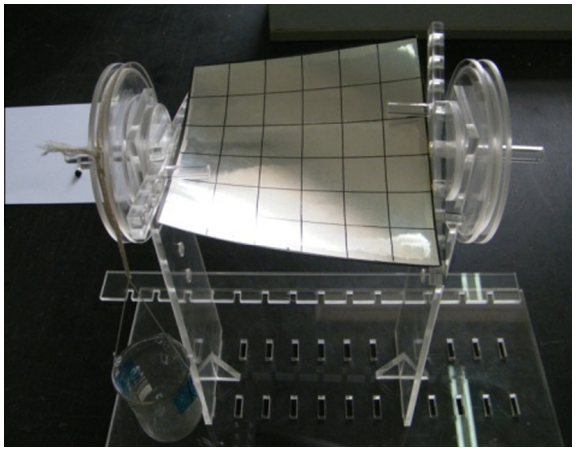

Fig. 4. The measurement for snapping twist moment.

snap-through process is simulated by applying loads such as force or moment to the edge of laminate. The analysis is performed using 4-node general purpose reduced integration shell elements (S4R) and geometrically non-linear algorithms (NLGEOM). The CFRP prepreg material studied is T300/QY8911 and the external isotropic layer is aluminum layer. The thermo-mechanical properties of these materials are listed in Table 1.

Slippage effects are simulated by the modification of the coefficients of thermal expansion from α_k to $\bar{\alpha}_k$ in accordance with Eq. (10). The effective thermal expansion in the fiber direction is given by $\mu\varepsilon_m^{cure}/2\Delta T$ and in the metal layer the effective thermal expansion coefficient in calculated using $\varepsilon_m^{cure}/\Delta T$. The thermal expansion transverse to the fiber direction remains unchanged. The reference-plane total strain in the metal layer at cure ε_m^{cure} can be determined by Eq. (9).

For this hybrid laminate studied in this paper, an imperfection must be introduced to finite element model to obtain the correct cured shape. Different imperfections can be used by changing material properties such as modulus and thermal expansion. The region where the imperfection is introduced has also important influence on the cured shape. The imperfection region used on the hybrid laminate is shown in Fig. 2. The two rectangular regions along the diagonal are chosen to introduce the imperfection on thermal expansion of aluminum layer, by changing the thermal expansion coefficient with the percentage of γ. The introduced imperfection is defined as $\alpha_{\text{imperfection}} = \alpha_m.(1 + \gamma)$.

4. Experiments

Within this work, several experimental investigations have been carried on laminates made of CFRP and aluminum. Three laminates were manufactured: $[0/90/Al]_T$ (100×100 mm, 150×150 mm, 300×50 mm), see Fig. 3. These hybrid laminates have been processed at a curing temperature of 180 °C and slowly cooled down to room temperature of 20 °C. It can be seen that the direction of the principal curvature is constantly 45°. The stable twisted shape is a cylindrical shell for square laminates. Two stable twisted shapes for rectangular laminate with size 300×50 mm are shown in Fig. 3. The laminates always deform towards the same side of x–y plane in two stable states.

The distance L between the two corner points of cylindrical shape and the deflection H are measured. The principal curvatures for square laminates can be calculated by the measured results, which are also presented in Fig. 3. For the rectangular laminate, it is difficult to directly calculate the curvature. The distances between the two corner points of twisted cylindrical shape and the deflection at the corner are measured to be 230 mm and 83 mm respectively.

To investigate the snap through behavior, a simple experiment was set up as shown in Fig. 4. The twist moment is applied to the edge of laminate by two cantilevers on the pulley. The distance between two cantilevers is 65 mm. The forces are recorded and the twist moments are obtained by multiplying the force by the distance. The critical twist moment snapping the laminate are measured to be 0.125 Nm for 100×100 mm [0/90/Al] laminate and 0.196 Nm for 150×150 mm. The twist moment is not obtained for rectangular laminate with size of 300×50 mm since the equipment fails to work to measure it.

5. Results

A series of bistable twisting hybrid laminates is analyzed to compare with the experimental measurements, and to begin examining how changes in geometry affect the shape. The changes of curvature shapes for various side-lengths are depicted by analytical, finite element model and experimental results in Fig. 5. These solutions are found using the analytical model presented in Section 2 accounting for slippage effects.

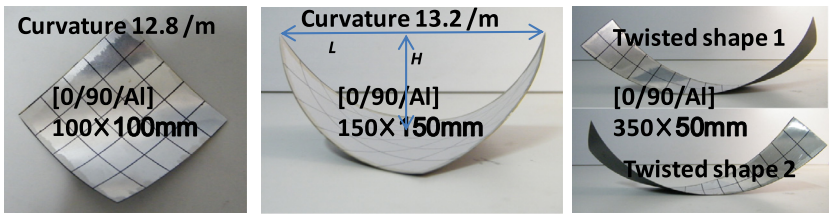

Fig. 3. Manufactured hybrid laminates.

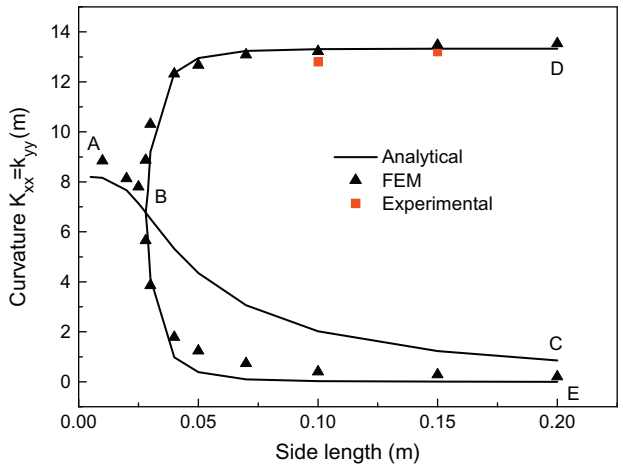

Fig. 5. Bifurcation diagram for a [0/90/Al] square laminate.

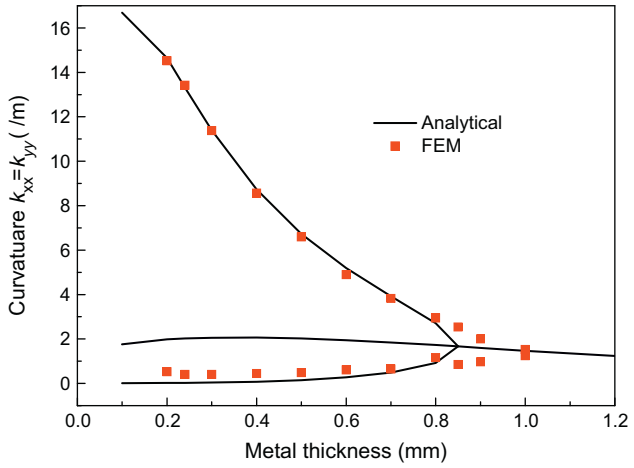

Fig. 6. Cured curvature vs. the metallic thickness for [0/90/Al] 100 × 100 mm square laminates.

Branch AB shows the curvature of the stable paraboloid shape which corresponds to the shape in Fig. 1b and occurs in the case of small laminates. The critical side length for the paraboloid shape is where the paraboloid shape becomes unstable, which defines the bifurcation point. After this bifurcation point, the paraboloid shape exists only theoretically as an unstable equilibrium state but not in reality indicated by the line BC. Instead of the paraboloid shape, two equivalent stable solutions (BD and BE) are calculated as the side length increases. An interesting result is that both principal curvatures in two stable states have the same sign instead of pure unsymmetric laminates and hybrid laminates with an inner isotropic layer. Branch BD represents the curvature a_0 of twisted cylindrical shape and the curvature b_0 of another twisted cylindrical shape. BE indicates the secondary curvature a_0 of twisted cylindrical shape and the secondary curvature b_0 of another twisted cylindrical shape, which asymptotically approach to zero with increasing side length. The finite element and experimental results are also plotted in Fig. 5 and found to be in close agreement with slippage coefficients of 0.2 applied to the aluminum hybrid laminates. The values of these slippage coefficients are selected on the basis of the experimentally observed laminate curvatures.

Fig. 6 plots the curve of curvatures vs. the metallic thickness. It is clear seen that the curvature increase as the metallic thickness decreases. For thin laminates, two stable twisted cylindrical shapes are observed, where the paraboloid shape is unstable. At a critical thickness, the bifurcation point is reached and only one stable paraboloid shape occurs instead of two cylindrical geometries form. The finite element solution correlates well with the analytical one before the bifurcation point. The finite element predicts a bifurcation point greater than that by analytical model. The analytical critical thickness is 0.85 mm but 1.0 mm by finite element.

Fig. 7 demonstrates three room temperature shapes after cooling down predicted by finite element analysis for 100 × 100 mm hybrid laminate. For the pure unsymmetric laminate and hybrid laminate with an inner metallic layer, finite element method predicts an unstable saddle shape without imperfection when the side length is larger, which coincide with the analytical solution. Although both analytical model and finite element method can give the unstable shape for the hybrid laminate, they are quite different in shape. The analytical model gives an unstable paraboloid shape with the equivalent curvature in two principal curvature directions, whereas the cured shape predicted by finite element method without imperfection introduced is a cylindrical shell, which is not in reality, as shown in Fig. 7a. Two stable twisted cylindrical shapes shown in Fig. 7b and c agree with the analytical prediction and the experimental results. The principal curvature direction is 45° with respect to the global axes.

In order to evaluate the effect of the imperfection magnitude, the 100 × 100 mm laminate is employed in order to evaluate the effect of the imperfection magnitude, as shown in Fig. 8. It shows that increasing imperfection tends to increase the cured curvature. The deviation at different imperfection from the average curvature is 13.76/m. The difference between minimum imperfection −5% and maximum imperfection 5% is 5.61%. It should be noted that too small imperfections, −1%, 0% and 1%, result in a cylindrical shape with the principal curvature direction along the global axes, which is unable to be observed in experiments. To check the change in curvature prediction induced by the slippage effect, the calculation on the 100 × 100 mm laminate is conducted again without the slippage effect and with 10% scatter of thermal expansion coefficient of aluminum ply. The results are shown in Fig. 9. It shows that the predicted curvatures with and without the slippage effect both vary linearly to the scatter of the aluminum thermal expansion coefficient. The experimental cured curvature is 12.8/m. The predicted curvature only considering the slippage effect is

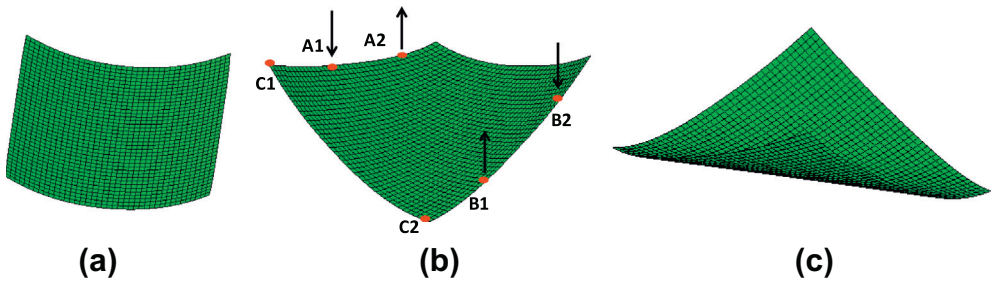

Fig. 7. Three room temperature shapes predicted by finite element analysis.

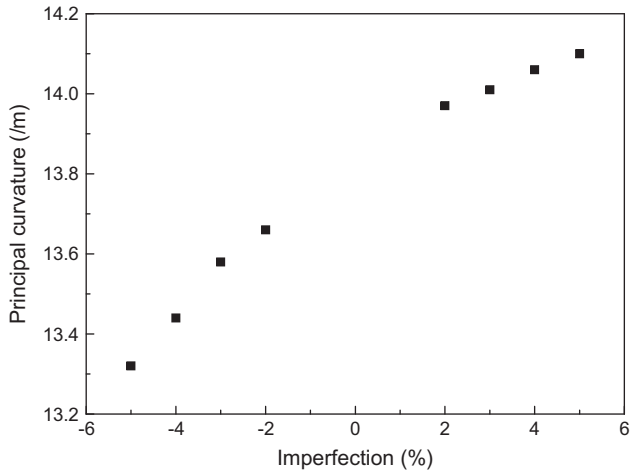

Fig. 8. Effects of imperfection magnitude on cured curvatures ($L_x = L_y = 100$ mm, $H = 0.49$ mm, $t = 0.24$ mm).

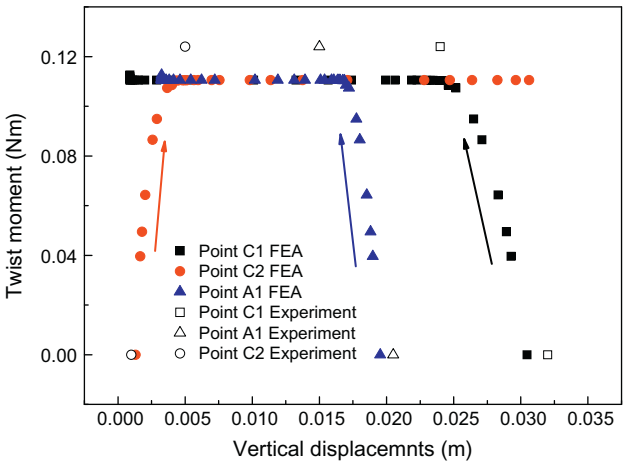

Fig. 11. Loads vs. displacements during snap through process for the [0/90/Al] 100 × 100 mm square laminate.

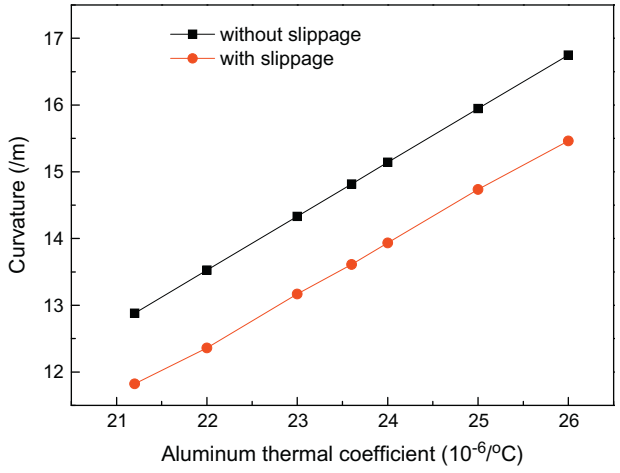

Fig. 9. Effects of slippage and thermal coefficient scatter on cured curvatures ($L_x = L_y = 100$ mm, $H = 0.49$ mm, $t = 0.24$ mm).

13.6/m, which leads to an error 6.3%. However, the predicted curvature without the slippage effect is 14.9/m, which leads to an error 16.4%. The predicted curvature by the model with the slippage effect is 10% less than that by the model without the slippage effect. If both considering the slippage and the scatter of thermal expansion (using the thermal expansion 5% less than the original model), the predicted cured curvature is 12.7/m, which is nearly consistent with the experimental result. Therefore, the change in curvature prediction should be the sum of the influences of slippage effect and the numerical scatter of original model.

Two stable shapes for 300 × 50 mm hybrid laminate are presented in Fig. 10. These shapes are consistent with the experimental shapes. The accurate characterization of these shapes may need the other technique, which is beyond this paper. The distance between two corner points from finite element analysis, as seen in Fig. 10a, is 223 mm and the experimental distance is 230 mm, which results in an error 3%. The predicted deflection is 85 mm and the measured deflection is 83 mm. It means finite element analysis predicts a larger curvature than the experimental curvature.

Finally, the snap though analysis is carried out on two laminates: 100 × 100 mm and 150 × 150 mm. In first analysis step, the laminate deforms to one of twisted shapes after cooling down. The cooling-down is simulated in first step and then second analysis step is restarted by applying twist moments to two edges. The loading scheme is indicated as in Fig. 7b, which matches with the experimental set-up. The simulated critical twist moment for 100 × 100 mm hybrid laminate is 0.115 Nm, which results in an error 8.0% compared with the experimental moment of 0.125 Nm. While the simulated critical moment for 150 × 150 mm hybrid laminate is 0.184 Nm, which has an error of 6.6% compared with the experimental one of 0.196Nm.

The load–displacement curve at points C1, C2 and A1 for 100 × 100 mm laminate are plotted in Fig. 11. All the initial displacements are obtained at the end of cooling down analysis, which is induced by thermal stress. It shows that the displacement at point C1 has an initial value of 30.6 mm and decreases to a very small value with the increase of loads. The initial displacement at point A1 is 19.5 mm and decreases with the increase of loads as well. In contrast to point C1, the displacement at point C2 increases as the load increases. The load gradually reaches to a critical value of 0.115 Nm. At this case, the displacements at three points change further although the load almost remains constant, which means that the collapse of laminate occurs at the critical load.

6. Conclusions

This paper presents a bistable twisting CFRP-metal hybrid laminate which has an external isotropic metallic layer. The investigation is focused on the hybrid laminate with layup [0/90/metal]$_T$.

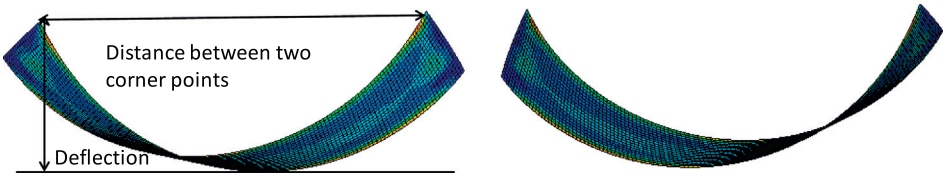

Fig. 10. Two stable shapes for 300 × 50 mm hybrid laminate predicted by finite element method.

The out-of-plane displacement of laminate has been solved analytically in the principal curvature coordinate system. Both the analytical and finite element models can capture two stable geometric and their predictions agree well with the experimental results. It is found that there exist three possible cure shapes: paraboloid, first twisted cylindrical and secondary cylindrical shapes. The laminate presented in this paper can be transformed from one negative curvature to another negative curvature. The principal curvature direction is shown to be 45° with respect to the global axes. The slippage effect is included in the analytical and numerical calculations, which has significant influence on the correct cure shape. An imperfection must be introduced to finite element model to obtain the correct cured shape. The two rectangular regions along the diagonal have been chosen to introduce the imperfection, which succeed to predict the correct shape. The snap through process have been investigated numerically and experimentally. The predicted snap-through loads correlate well with experimental results.

Acknowledgements

This work was supported by National Natural Science Foundation of China [Grant No. 10872058], the Major State Basic Research Development Program of China (973 Program) [Grant No. 2010CB631100], and the Laboratory of Science and Technology on Advanced Composites in Special Environments.

References

[1] Hufenbach W, Gude M, Czulak A. Actor-initiated snap-through of unsymmetric composites with multiple deformation states. J Mater Process Technol 2006;175:225–30.
[2] Schutz MR. A concept for Airfoil-like active bistable twisting structures. J Intell Mater Syst Struct 2008;19(2):157–69.
[3] Daynes S, Weaver PM, Potter KD. Aeroelastic study of bistable composite airfoils. J Aircraft 2009;46(6):2169–73.
[4] Lachenal X, Weaver PM, Daynes S. Multi-stable composite twisting structure for morphing applications. Proc. R. Soc. A. doi: http://dx.doi.org/10.1098/rspa.2011.0631.
[5] Lei YM, Yao XF. Experimental study of bistable behaviors of deployable composite structure. J Reinf Plast Compos 2010;29:865–73.
[6] Hyer MW. The room-temperature shapes of four-layer unsymmetric cross-ply laminates. J Compos Mater 1982;16(4):318–40.
[7] Jun WJ, Hong CS. Effect of residual shear strain on the cured shape of unsymmetric cross-ply thin laminates. Compos Sci Technol 1990;38:55–67.
[8] Pirrera A, Avitabile D, Weaver PM. Bistable plates for morphing structures: a refined analytical approach with high-order polynomials. Int J Solids Struct 2010;47:3412–25.
[9] Hyer MW. Calculations of the room-temperature shapes of unsymmetric laminates. Compos Mater 1981;15:296–310.
[10] Tawfik SA, Stefan DD, Armanios E. Planform effects upon the bistable response of cross-ply composite shells. Composites Part A 2011;42:825–33.
[11] Giddings PF, Bowen CR, Salo AIT, et al. Bistable composite laminates: effects of laminate composition on cured shape and response to thermal load. Compos Struct 2010;92:2220–5.
[12] Cho M, Kim MH, Choi HS, et al. A study on the room-temperature curvature shapes of unsymmetric laminates including slippage effects. J Compos Mater 1998;32(5):460–82.
[13] Harper BD. The effects of moisture induced swelling upon the shapes of anti-symmetric cross-ply laminates. J Compos Mater 1987;21:36–48.
[14] Jun W, Hong C. Cured shape of unsymmetric laminates with arbitrary lay-up angles. J Reinf Plast Compos 1992;11:1352.
[15] Etches J, Potter K, Weaver P, Bond I. Environmental effects on thermally induced multistability in unsymmetric composite laminates. Compos A: Appl Sci Manuf 2009;40:1240–7.
[16] Gigliotti M, Jacquemin F, Molimard J, et al. Transient and cyclical hygrothermoelastic stress in laminated composite plates: modelling and experimental assessment. Mech Mater 2007;39(8):729–45.
[17] Gigliotti M, Wisnom MR, Potter KD. Loss of bifurcation and multiple shapes of thin [0/90] unsymmetric composite plates subject to thermal stresss. Compos Sci Technol 2004;64:109–28.
[18] Gigliotti M, Minervino M, Grandidier JC, Lafarie-Frenot MC. Predicting loss of bifurcation behaviour of 0/90 unsymmetric composite plates subjected to environmental loads. Compos Struct 2012;94:2793–808.
[19] Hufenbach W, Gude M, Kroll L. Design of multistable composites for application in adaptive structures. Compos Sci Technol 2002;62:2201–7.
[20] Schultz MR, Hyer MW, Williams RB, et al. Snap-through of unsymmetric laminates using piezocomposite actuators. Compos Sci Technol 2006;66:2442–8.
[21] Tawfik SA, Stefan DD, Armanios E. Unsymmetric composite laminates morphing via piezoelectric actuators. Composites Part A 2011;42:748–56.
[22] Giddings PF, Kim HA, Salo AIT, Bowen CR. Modelling of piezoelectrically actuated bistable composites. Mater Lett 2011;65:1261–3.
[23] Vogl GA, Hyer MW. Natural vibration of unsymmetric cross-ply laminates. J Sound Vib 2011;330:4764–79.
[24] Arrieta AF, Neild SA, Waggb DJ. On the cross-well dynamics of a bi-stable composite plate. J Sound Vib 2011;330:3424–41.
[25] Bowman Jason, Sanders Brian, Bryan Cannon. Development of next generation morphing aircraft structures. In: 48th AIAA/ASME/ASCE/AHS/ASC structures, structural dynamics, and materials conference. Honolulu, Hawaii, April, 2007.
[26] Dai FH, Zhang BM, Du SY. A novel bistable hybrid composite laminate. In: 17th International conference on composite materials (ICCM-17). Edinburgh, UK, July, 2009.
[27] Daynes S, Weaver PM. Analysis of unsymmetric CFRP–metal hybrid laminates for use in adaptive structures. Composites Part A 2010;41:1712–8.